Polymer Composites

WILEY | spe INSPIRING PLASTICS PROFESSIONALS

RESEARCH ARTICLE OPEN ACCESS

Analysis of Electrical Conductivity in Chopped Carbon Fiber/High-Density Polyethylene Composites Under Tensile Alignment: Experimental and Simulation Approaches

Gu-Hyeok Kang[1] | Myungsoo Kim[2] | Young-Bin Park[3,4]

[1]Department of Mechanical Engineering, Kangwon National University, Samcheok-si, Gangwon State, Republic of Korea | [2]Department of Mechanical and Automotive Engineering, Youngsan University, Yangsan-si, Gyeongsangnam-do, Republic of Korea | [3]Ulsan National Institute of Science and Technology (UNIST), Ulsan, Republic of Korea | [4]Fraunhofer Innovation Platform for Composites Research @ UNIST, Ulsan, Ulju-gun, Republic of Korea

Correspondence: Myungsoo Kim (mskim@ysu.ac.kr) | Young-Bin Park (ypark@unist.ac.kr)

Received: 13 May 2025 | **Revised:** 21 July 2025 | **Accepted:** 2 August 2025

Funding: This research was supported by the K-Carbon Flagship R&D Program (Grant No. RS-2024-00417957) funded by the Ministry of Trade, Industry and Energy (MOTIE) of Korea through the Korea Evaluation Institute of Industrial Technology (KEIT) by the National Research Foundation of Korea (NRF) funded by the Ministry of Science and ICT (MSIT) (Grant No. 2021R1F1A1051836) by the National Research Council of Science and Technology (NST) grant funded by MSIT (Grant No. CRC23011-000) and by the Korea Institute of Marine Science & Technology Promotion (KIMST) funded by the Ministry of Oceans and Fisheries (2520000449).

Keywords: chopped carbon fiber | draw ratio | electrical conductivity | fiber alignment | high-density polyethylene composite | percolation theory

ABSTRACT

The low electrical conductivity of polymer-based composites limits their applicability to electromagnetic interference shielding in the automotive industry. This study aimed to enhance the electrical conductivity of composites composed of chopped carbon fiber (CCF) and high-density polyethylene (HDPE). Composite samples of CCF/HDPE were fabricated using a take-up machine, which used a unique tension alignment method following extrusion. The impact of various manufacturing variables, such as fiber content, length, and draw ratio (DR), on electrical conductivity was examined. The highest conductivity measured was 2.808 S/cm for CCF with a length of 1 mm, 10 wt%, and a DR of 2. In addition, percolation theory was utilized to compare and predict the effects of these manufacturing variables. Electrical conductivity improved as the length, content, and DR of the CCF increased. The experiments were simulated considering both CCF entanglement and alignment. The findings revealed a significant increase in electrical conductivity with a higher CCF weight percentage and DR surpassing the percolation threshold. The higher DR aided in aligning the fibers, resulting in enhanced electrical conductivity in the aligned direction. Furthermore, electrical conductivity was enhanced as the length of the CCF decreased.

1 | Introduction

Extensive studies have been conducted on electromagnetic interference (EMI) shielding, particularly in the automotive industry [1–11]. Following research on electrically conductive composite materials [1–6], several studies have focused on structural composites in EMI shielding applications [7]. One promising approach involves the alignment of chopped carbon fibers (CCFs) within composite materials to enhance their mechanical properties and electrical conductivity [12–17]. This method lays the foundation for developing structural composites for electric vehicle components, such as underbody shields and battery enclosures, utilizing advanced composite materials [18–21].

CCFs are an ideal reinforcement material for structural composites in electric vehicles owing to their superior electrical conductivity and mechanical strength. Improvements in both properties have been observed in composites in which CCFs

Summary

- Innovative post-extrusion tension alignment method enhances electrical conductivity.
- Predictive percolation model based on fiber content, fiber length, and draw ratio.
- Entanglement analysis of chopped carbon fiber with varying lengths.

are combined with thermoplastic polymers [12, 22]. Composites can achieve more efficient electrical conductivity in a specific direction by applying a force to align the CCF during the manufacturing process. This alignment process has demonstrated significant potential for enhancing the electrical conductivity of composite materials, making them an appealing choice for applications in electric vehicles, such as EMI shielding or thermal runaway prevention in batteries caused by electrical overload.

Recent studies have used electromagnetic forces, such as magnetic or electric fields, to align the CCF [13, 14] as well as mechanical alignment methods, such as repeated stretching using a rotating drum and nozzle [15].

However, these methods can be costly; are limited to specific fiber types; and may not be suitable for high-viscosity thermoplastics. In this study, a novel approach is proposed for CCF alignment within high-viscosity thermoplastic composites via mechanical pulling, with the aim of improving the electrical conductivity [22, 23].

This study investigates the enhanced electrical properties of unidirectionally aligned CCF/high-density polyethylene (HDPE) composites, particularly for applications requiring unidirectional electrical conductivity. Experiments were conducted to measure and analyze the electrical conductivity of the composites with varying fiber contents, lengths, and draw ratios (DRs) using a post-extrusion tensile alignment method. Percolation theory was applied to analyze the electrical conductivity from different perspectives. Electrical conductivity curves based on the CCF content were constructed by fitting the percolation model to the experimental results. In addition, the effects of the DR and CCF length on the patterns of the conductivity curves and percolation threshold were examined. This study provides insight into the changes in the electrical performance of composites as a function of the fiber content, length, and tensile force. These findings are important for optimizing composite design and gaining a deeper understanding of electrical conductivity in such materials.

2 | Experimental Procedure

2.1 | Materials

CCF (SYC-TR-PU, Sunyoung Industry, Yangsan, Korea) and HDPE (HDPE B230A, Hanwha Total, Seosan, Korea) were used for the tensile experiments. CCF fibers treated with polyurethane (PU) sizing were prepared, with lengths of 1, 3, 6, and 12 mm and a density of 1.78 g/cm^3. The diameter of the CCF provided by the manufacturer was 6.97 μm, resulting in aspect ratios of 143, 430, 861, and 1722, respectively. The HDPE had a density of 0.963 g/cm^3 and a molecular weight of 50,000.

2.2 | Processing

The CCFs were supplied in pellet form and contained a PU binder. The PU binder was removed using acetone during bath sonication. Subsequently, the exfoliated fibers were dried in a high-temperature vacuum oven (80°C, 0.05 bar) for 8 h, while the HDPE was dried under the same conditions for 6 h.

Extrusion was carried out using an OC-200 extruder (Ocean Co. Ltd.) that was equipped with a 6 mm diameter die. Take-up rolls were installed at the end of the extrusion line to apply controlled tension, and the extrudate was cooled in a water bath to form filament-shaped composites. Tension was applied by adjusting the DRs to 1, 1.5, and 2 between the first and second take-up rolls; as illustrated in Figure 1. The filament diameter after the water bath was measured to confirm the applied DRs.

For experimental sampling, the filament-shaped composites that were collected once the extrusion process had stabilized were transformed into flat plates by unidirectionally aligning the filaments and utilizing a heating press and mold to fabricate flat plates (150 mm × 150 mm). Samples for the electrical conductivity tests were prepared using a water jet.

2.3 | Characterization

The volumetric electrical resistivity of the samples was calculated following the two-probe method specified in ASTM D4496. In this method, a known DC voltage is applied across two electrodes that are placed on the sample surface, and the current passing through the material is measured. Thereafter, the volumetric resistivity was calculated using the measured resistance, cross-sectional area, and distance between the electrodes. Unidirectionally aligned specimens were prepared to assess the electrical conductivity of the oriented composites.

Four samples were tested for each formulation using a Keithley 2002 multimeter with the two-probe configuration. This method offers a simple and effective approach for evaluating anisotropic composite samples. The volumetric electrical resistivity was calculated as follows:

$$\mathrm{ER} = \frac{\Delta V \times w \times t}{i \times L} \tag{1}$$

where ER represents the volume electrical resistivity (Ω cm), ΔV represents the voltage drop over the length of the sample (V), w represents the sample width (1.27 cm), t represents the sample thickness (0.33 cm), i represents the current (A), and L represents the length over which ΔV is measured (6 cm).

2.4 | Model for Electrical Conductivity

The experimental results were analyzed using percolation theory to examine the behavior and variation in the electrical

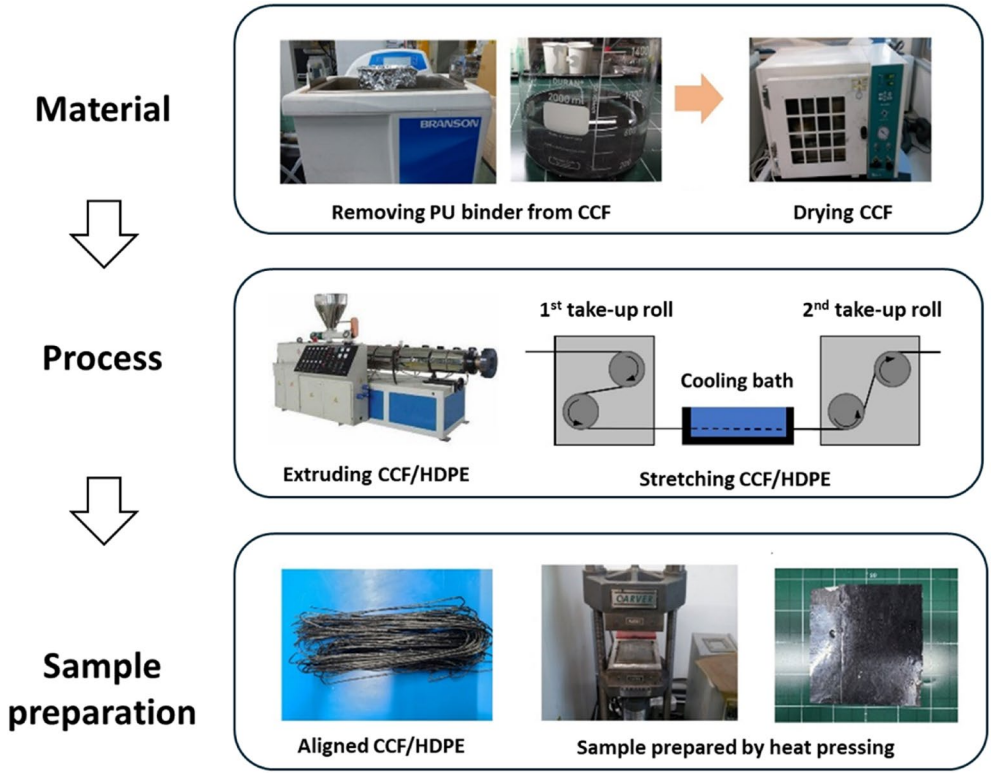

FIGURE 1 | Manufacturing process of the CCF/HDPE composites.

conductivity of the CCF/HDPE composites based on the CCF content. This theory is represented by a power-law equation that illustrates the relationship between the electrical conductivity of composites and the volume fraction of conductive fillers [24–29].

$$\sigma = \sigma_f \left(V_f - V_{fp}\right)^t \tag{2}$$

where σ represents the electrical conductivity of the composite, σ_f represents the electrical conductivity of the filler, and V_f represents the filler volume fraction. This equation is valid for volume fractions higher than V_{fp}, which represents the filler volume fraction at the percolation threshold. In cases in which fillers are discontinuous particles, such as chopped fibers or spherical particles, σ_f can be adjusted owing to the presence of tunneling barriers that are associated with the polymer matrix [27].

The critical exponent, denoted as t, typically falls within the range of 1.6–1.9 for a three-dimensional system [25–29]. However, its value can be 2, 3, or even higher owing to factors such as special geometries, tunneling effects, and the coalescence of conducting particles [26–32].

The typical shape of the electrical conductivity plot drawn using Equation (2) is shown in Figure 2. As the filler volume fraction increases beyond the percolation threshold, two distinct zones emerge: the transition and conduction zones. The dotted circle in Figure 2 was identified as the "inflection region" in this study.

A low value of the critical exponent t resulted in a rapid increase in the electrical conductivity in the transition zone with

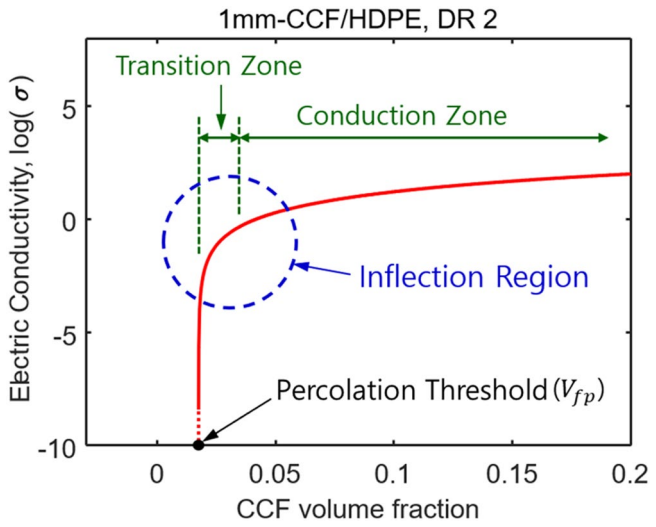

FIGURE 2 | Electrical conductivity curve (obtained from the fitting results for 1 mm-CCF/HDPE with a DR of 2).

an increasing V_f as the value of $\left(V_f - V_{fp}\right)$ fell between 0 and 1. Furthermore, the conductivity curve changed abruptly in the inflection region and then quickly plateaus. That is, if t was large, the electrical conductivity in the transition region increased slowly and then leveled off slowly with an increase in V_f.

The coefficients σ_f, V_{fp}, and t of the electrical conductivity model had to be determined to derive Equation (2). This process involved first identifying the percolation threshold V_{fp} through trial and error based on the available data. Subsequently, σ_f and

t were determined by establishing trend lines using the obtained V_{fp}. Equation (2) was modified to obtain the percolation threshold, with Equation (3) resulting from taking the logarithm of both sides.

$$\log \sigma = \log \sigma_f + t \log\left(V_f - V_{fp}\right) \tag{3}$$

Equation (6) could be obtained using the ith and jth electrical conductivity in Equations (4) and (5) obtained experimentally.

$$\log \sigma_i = \log \sigma_f + t \log\left(V_{fi} - V_{fp}\right) \tag{4}$$

$$\log \sigma_j = \log \sigma_f + t \log\left(V_{fj} - V_{fp}\right) \tag{5}$$

$$\log \sigma_i - log\sigma_j = t\left\{log\left(V_{fi} - V_{fp}\right) - log\left(V_{fj} - V_{fp}\right)\right\} \tag{6}$$

Thus, the V_{fp} value that minimizes EV in Equation (7) was obtained through trial and error, as follows:

$$\mathrm{EV} = \frac{\log \sigma_i - log\sigma_j}{\log \sigma_m - log\sigma_n} - \frac{\left\{\log\left(V_{fi} - V_{fp}\right) - \log\left(V_{fj} - V_{fp}\right)\right\}}{\left\{\log\left(V_{fm} - V_{fp}\right) - \log\left(V_{fn} - V_{fp}\right)\right\}} \tag{7}$$

where i, j, m, and n are random numbers that represent certain experiments. Among these, two random numbers can be identical (e.g., $i = m$).

In the process of determining the V_{fp} value through trial and error, the EV value was calculated by incrementing V_{fp} by 1.0e-6 from 0 (0%) to 0.5 (50%) to identify the value that minimized the absolute value of EV. Theoretically, the EV value must be zero at the optimal V_{fp}; however, this is not the case in practice.

Once V_{fp} was obtained, the $\log \sigma_f$ and t values were recalculated using the experiment results and trend line estimation method. That is, Equation (3) can be rewritten as follows:

$$y = a + bx \tag{8}$$

where y, a, b, and x denote $\log \sigma$, $\log \sigma_f$, t, and $\log\left(V_f - V_{fp}\right)$, respectively. That is, the coefficients of $a\ (= \log \sigma_f)$ and $b\ (= t)$ that minimize the error with the experimental results were determined using the least-squares fitting method. In this study, the "polyfit" function in Matlab was utilized to obtain these coefficients. Further details on obtaining the coefficients can be found in [33, 34].

The volume fraction (V_f) of CCF had to be obtained to calculate the aforementioned equations. Because the amount of CCF was determined based on weight ratios (2.5, 5, 7.5, and 10 wt%) in the experiment, it was necessary to convert the values into volume ratios. Equation (9) was employed for this purpose [35].

$$V_f = \frac{W_f}{W_f + \left(\rho_f / \rho_m\right) - \left(\rho_f / \rho_m\right) W_f} \tag{9}$$

where W_f represents the weight ratio of the CCF, and ρ_f and ρ_m represent the densities of the CCF and HDPE, respectively. The manufacturer-provided values for ρ_f and ρ_m (1.78 and 0.963 g/cm^3, respectively) were utilized.

3 | Results and Discussion

3.1 | Electrical Conductivity Versus Weight Percentage, CCF Length, and DR

The electrical conductivity results of the CCF/HDPE composites are presented in Figure 3 and Table 1. In this study, CCF lengths of 1, 3, 6, and 12 mm were utilized, with different DRs set. The weight percentages of CCF in the composites were 2.5, 5, 7.5, and 10 wt%, which were determined based on the input. Unfortunately, the sample of 12 mm-CCF/HDPE at DR 2 could not be produced owing to high viscosity hindering elongation.

The findings revealed a direct correlation between the electrical conductivity and CCF content, following a percolation theory curve that is commonly observed in composite materials with conductive fillers. A significant increase in the electrical conductivity was observed for all CCF lengths starting from 5 wt%; with a notable spike at 7.5 wt%, followed by a gradual increase up to 10 wt% which is consistent in previous studies [36, 37].

A rheological analysis of the composites is necessary for a better understanding of the processing behavior. Rheological measurements can provide valuable insights into the viscoelastic properties of the polymer matrix with varying CCF lengths and loadings, particularly in relation to the difficulty in processing the 12-mm-CCF/HDPE composite at DR 2, as well as the behavior of other composite configurations.

The observed behavior is consistent with that in previous studies on fiber-reinforced thermoplastics, in which increased fiber content and longer fiber lengths contributed to shear thinning but also caused processing challenges owing to fiber entanglement and poor stress transfer at high deformation rates [38, 39]. A detailed rheological study is planned as part of future work.

The diameter of the extrusion hole in the extruder that was used in the sample manufacturing process was 6 mm, leading to the potential entanglement of CCFs in the 12-mm-CCF sample owing to the length exceeding the hole diameter. Consequently, the anticipated enhancement in the properties of samples from longer CCF lengths is expected to be minimal.

As shown in Figure 3, the electrical conductivity tended to increase as the length of the CCF decreased and the CCF content and DR increased. To provide a more intuitive comparison of electrical conductivity, the values were normalized between 0 and 1, as shown in Figure 4. Figure 4a shows the relationship between the normalized electrical conductivity and CCF weight percentage. The process of determining the normalized electrical conductivity is outlined in Appendix A, with normalization performed for CCFs of varying lengths. As shown in Figure 4a, the electrical conductivity exhibited an increase with an increase in the CCF weight percentage.

The relationship between the length of the CCF and normalized electrical conductivity (refer to Appendix B for details on the normalization) is shown in Figure 4b. The composites exhibited

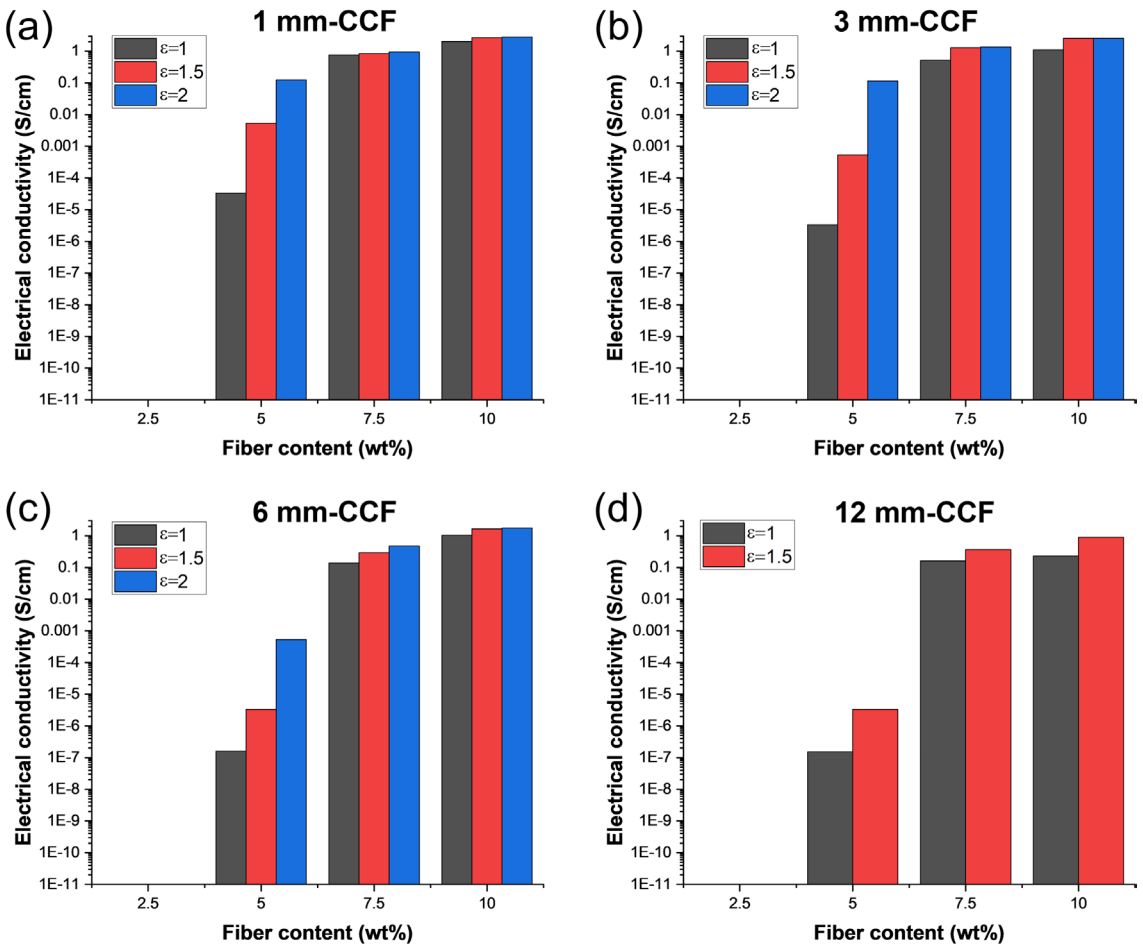

FIGURE 3 | Results of electrical conductivity as a function of DRs, weight percentages (2.5, 5, 7.5, and 10 wt%), and CCF lengths: (a) 12 mm, (b) 6 mm, (c) 3 mm, and (d) 1 mm.

higher electrical conductivity as the CCF length decreased. Prior to the experiment, the composites were expected to show higher electrical conductivity with an increase in length. However, contrary to expectations, the electrical conductivity decreased with an increasing length. This unexpected outcome can be attributed to the reduced gap between reinforcements as the volume decreased while maintaining the same filler content within the composite. A conceptual diagram to aid in understanding this concept is shown in Figure 5. In Figure 5a,b, the circular fillers have identical areas. Because the diameter of the small circle in Figure 5a is half that of the large circle in Figure 5b, the total area of the fillers remains the same. However, Figure 5a has a considerably smaller gap between the circles owing to their small diameter. When this concept is expanded to three dimensions and applied to the same amount of CCF, a CCF with a short length has a relatively small volume; therefore, the gap between the short CCFs is expected to be considerably smaller. Consequently, it can be inferred that the electrical conductivity is enhanced as the tunneling effect between the discontinuous CFs decreases.

The relationship between the DR and normalized conductivity is shown in Figure 4c. Notably, the DR 2 sample was not ready for the 12 mm-CCF/HDPE sample. The electrical conductivity increased as the DR increased. This phenomenon can be attributed to the enhanced alignment of the CCF in the longitudinal direction owing to increased tensile force during the manufacturing process, resulting in enhanced electrical conductivity in the longitudinal direction.

In summary, the electrical conductivity in the longitudinal direction, which is the tensile direction, increased with a higher CCF content, a shorter CCF length, and an increased DR.

3.2 | Percolation Theory

The percolation thresholds (V_{fp}) obtained using Equation (7) are shown in Table 2 and Figure 6.

As shown in Figure 6a, the percolation threshold decreased significantly as the DR increased for the 1 mm-CCF sample. Although the difference was not significant for samples with varying CCF lengths, the threshold decreased with higher DRs. A lower threshold indicates higher electrical conductivity, suggesting that a small amount of CCF can result in high electrical conductivity. The increase in the DR led to improved alignment of the CCF in the longitudinal direction, resulting in a reduced electrical conductivity threshold. In Figure 6b, the threshold values for all samples were similar at DR 1. At DR 1.5, the threshold value for the 1 mm-CCF sample was lower than that for the other CCF samples, although

TABLE 1 | Electrical conductivity results (unit: S/cm).

Composite samples	CCF wt.%	DR		
		1	1.5	2
1 mm	2.5	0	0	0
	5	3.35E-05	0.00535	0.12291
	7.5	0.75904	0.83859	0.95141
	10	2.04482	2.67597	2.80794
3 mm	2.5	0	0	0
	5	3.35E-06	5.35E-04	0.11425
	7.5	0.51674	1.27563	1.34648
	10	1.10243	2.54042	2.56295
6 mm	2.5	0	0	0
	5	1.52E-07	3.35E-06	5.35E-04
	7.5	0.13676	0.29401	0.47294
	10	1.03248	1.65845	1.74888
12 mm	2.5	0	0	—
	5	1.52E-07	3.35E-06	—
	7.5	0.16173	0.37076	—
	10	0.22819	0.89406	—

not significantly. However, at DR 2, the threshold value decreased as the CCF length decreased. As mentioned previously, a small threshold value indicates an improvement in electrical conductivity. Specifically, the electrical conductivity of the shortest 1-mm-CCF sample demonstrated the most significant improvement. This indicates that, as the length of the CCF increases, more tangles between CCFs will occur [40], hindering alignment in the longitudinal direction during the drawing process.

That is, shorter 1-mm-CCFs are expected to have fewer tangles between them, allowing for better alignment during the drawing process. Schematics of the CCF distribution in two dimensions with different lengths within the composites are shown in Figure 7. Short CCFs with low aspect ratios and long CCFs with high aspect ratios are shown in Figure 7a,b, respectively.

TABLE 2 | Percolation threshold V_{fp} obtained using the trial-and-error method.

	1-mm-CCF/HDPE	3-mm-CCF/HDPE	6-mm-CCF/HDPE	12-mm-CCF/HDPE
DR 1	0.027674	0.027685	0.027561	0.027686
DR 1.5	0.026898	0.027681	0.027541	0.027685
DR 2	0.017793	0.026468	0.027277	—

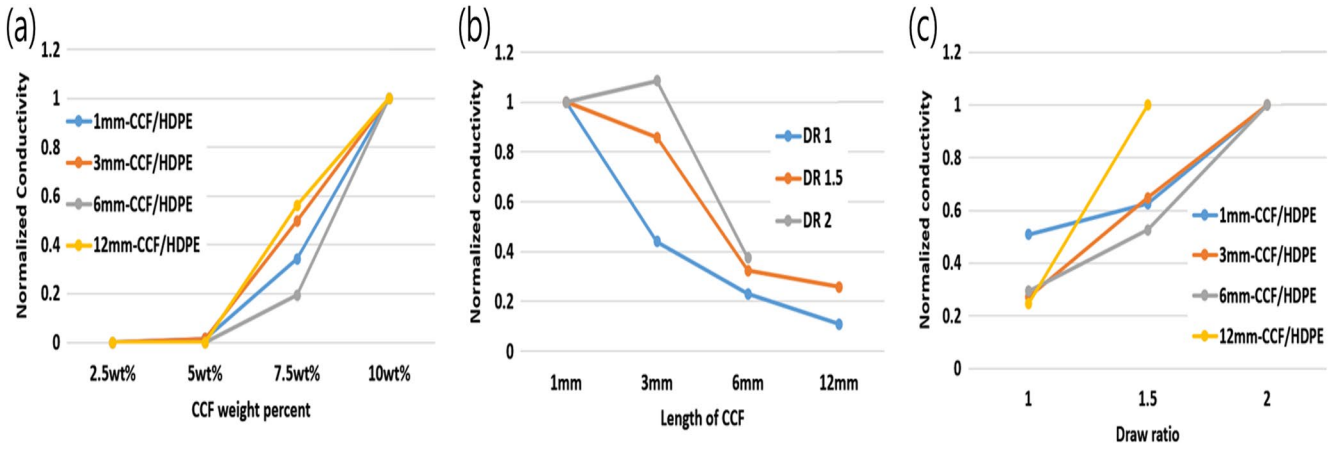

FIGURE 4 | Normalized conductivities of the composites in terms of (a) CCF wt%, (b) CCF length, and (c) DR.

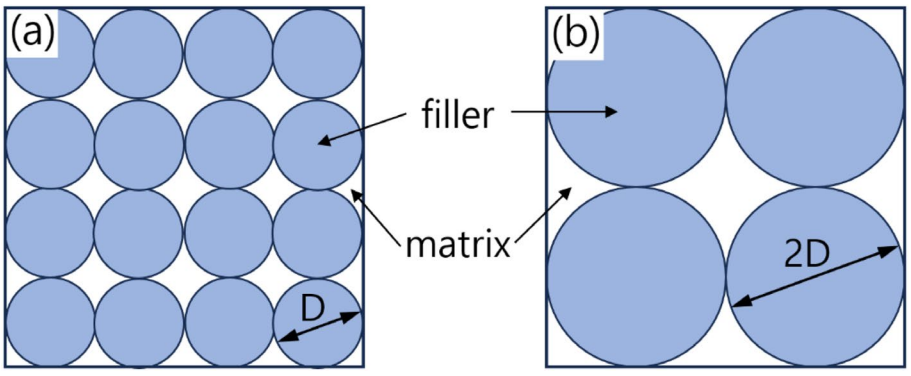

FIGURE 5 | Conceptual diagram of fillers with different areas or volumes with the same contents.

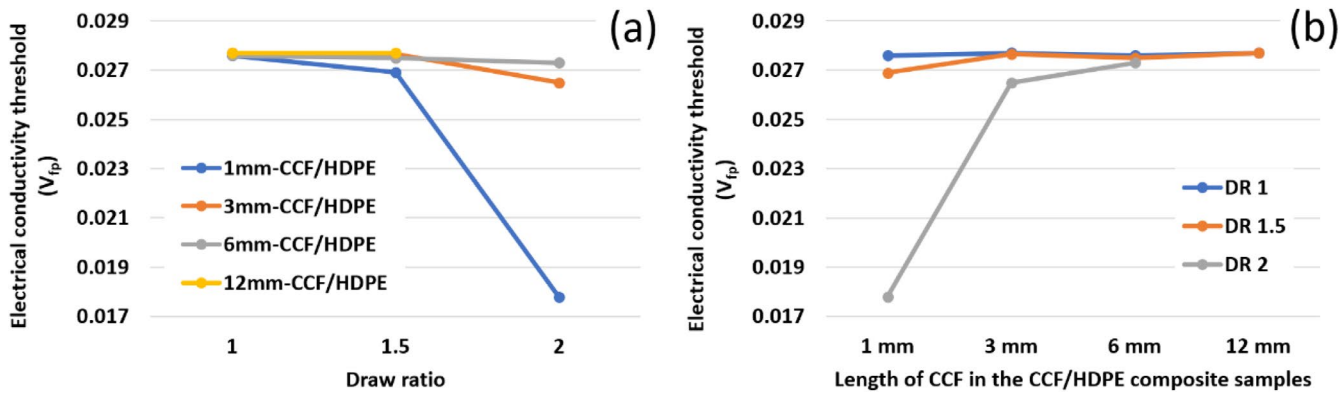

FIGURE 6 | Percolation thresholds of electrical conductivity (V_{fp}): (a) thresholds versus DRs and (b) thresholds versus CCF lengths.

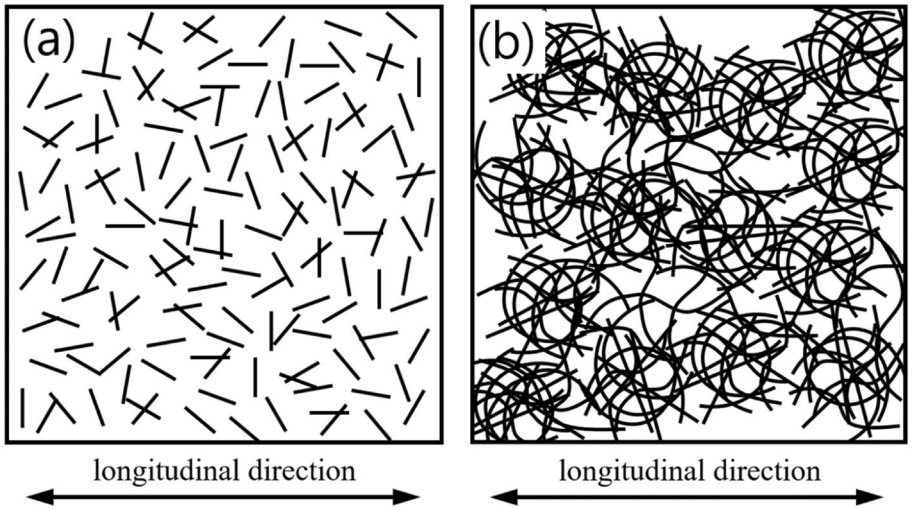

FIGURE 7 | CCF distribution patterns in the polymer composites: (a) short CCFs and (b) long CCFs.

Notably, CCFs may not only exist in these two extreme cases. Short CCFs are likely to exist in the form shown in Figure 7a, whereas long CCFs are expected to be similar to those shown in Figure 7b within composites. When subjected to tensile loads, the CCFs in Figure 7a are more likely to align along the longitudinal direction, whereas the tangled parts in Figure 7b are expected to impede rearrangement under tensile loads.

Scanning electron microscopy (SEM) images of the fracture surfaces of the CCF/HDPE composite samples are shown in Figure 8. The 1-mm-CCF sample (short CCF sample) in Figure 8a appears less entangled than the 12-mm-CCF sample (long CCF sample) in Figure 8b; as explained in Figure 7.

Figure 8a,c show the SEM images of the 1-mm-CCF 10 wt%/HDPE sample, where (a) and (c) present images with a DR of 1 and 2, respectively. In Figure 8a, the CCFs are aligned in various directions; however, most CCFs in Figure 8c are aligned in a single direction. In summary, the alignment of the CCFs in the sample increased because of the increase in the DR, leading to improved electrical conductivity of the composite samples. Conversely, the 12-mm-CCF 10 wt%/HDPE samples are shown in Figure 8b,d, with the CCFs in both images randomly oriented. Despite Figure 8d having a DR of 1.5, unlike Figure 8c, the increased alignment of CCFs cannot be attributed to the increased DR. As shown in Figure 7, the entanglement of CCFs may impede alignment improvement.

σ_f theoretically refers to the electrical conductivity of filler. In the case of electrical conductivity in unidirectional continuous fiber composites along the longitudinal direction, the value remains constant regardless of the DR. However, CCF is discontinuous in composites. Although the electrical conductivity of CCF itself is crucial in determining the overall composite conductivity, the contact between adjacent discontinuous CCFs and the gaps between adjacent CCFs that are not in contact will have more significant effects on the determination of σ_f. That is, the value of σ_f may vary depending on the composite manufacturing and measurement methods.

As shown in Table 3, $\log \sigma_f$ increased as DR increased for the 1-mm-CCF/HDPE sample and it decreased for the other CCF/HDPE samples with the other CCF lengths. The variations in $\log \sigma_f$ can be interpreted as changes in electrical conductivity surrounding the filler. Composites containing short (1 mm) CCF are typically distributed as shown in Figure 7a, with the CCF properly aligning owing to an increase in the DR, resulting in an increase in DR and probably increasing the value of $\log \sigma_f$. Conversely, composites with CCF lengths of at least 3 mm may be distributed similarly to those shown in Figure 7b, potentially

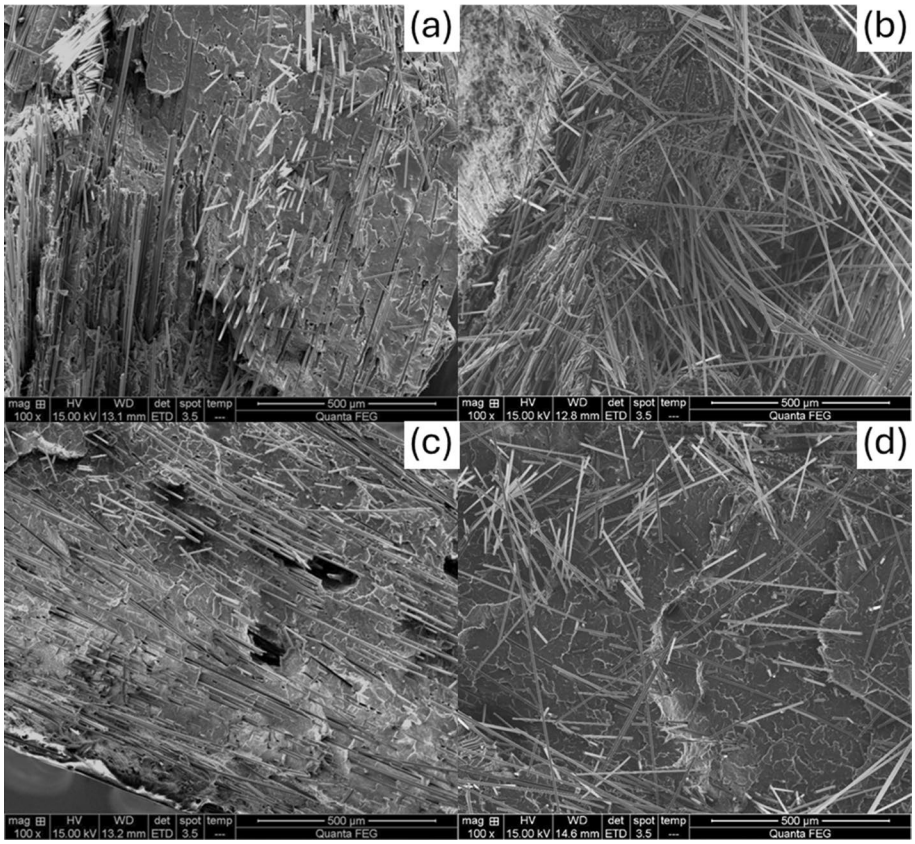

FIGURE 8 | SEM images of the CCF/HDPE composite samples: (a) 1 mm-CCF, 10 wt%, DR 1; (b) 12 mm-CCF, 10 wt%, DR 1; (c) 1 mm-CCF, 10 wt%, DR 2; and (d) 12 mm-CCF, 10 wt%, DR 1.5.

TABLE 3 | $\log \sigma_f$ obtained using least-squares fitting.

	1-mm CCF/ HDPE	3-mm CCF/ HDPE	6-mm CCF/ HDPE	12-mm CCF/ HDPE
DR 1	1.413682	1.233580	2.885379	1.4034390
DR 1.5	1.710699	0.975368	2.472056	1.3013741
DR 2	2.28468	0.968453	1.892419	—

impeding CCF alignment in the longitudinal direction as the DR increases. That is, the gaps between the CCF agglomerations increase with an increase in tensile force, probably resulting in a decreasing $\log \sigma_f$ for the samples with long CCFs. In terms of the impact of the CCF length on $\log \sigma_f$, the 6-mm-CCF/HDPE sample exhibited the highest $\log \sigma_f$ values at DR 1 and 1.5, whereas the 1-mm-CCF/HDPE sample exhibited the highest value at DR 2. Overall, the influence of the CCF length on $\log \sigma_f$ did not demonstrate a consistent trend.

The variable t represents the exponential value in Equation (2). As elucidated in Section 2.4, a small t value indicates a rapid increase in the electrical conductivity curve with respect to the CCF content exceeding the threshold value, followed by a rapid flattening in the inflection region. Essentially, as the t value increased, the electrical conductivity gradually flattened in the inflection region after an increase in the transition zone (Figure 9a).

As shown in Table 4, t increased as the DR increased for the 1 mm-CCF/HDPE sample but decreased for the 6 mm-CCF/HDPE sample. Furthermore, the 1-mm-CCF and 6-mm-CCF samples showed higher values compared with the 3-mm-CCF and 12-mm-CCF samples. However, a consistent trend was difficult to discern.

As mentioned previously, the percolation threshold V_{fp} was initially determined, followed by σ_f and t by establishing trend lines to derive the percolation theory curve, as shown in Figure 9. The electrical conductivity curves prepared using Equation (2) based on the electrical conductivity experimental results of the 1, 3, 6, and 12-mm-CCF/HDPE samples are shown in Figure 9a,c,e,f, respectively, whereas the results of the least-squares fitting to obtain $\log \sigma_f$ and t in Equations (3) and (8), which were utilized to draw the curves in Figure 9a,c,e,f, are shown in Figure 9b,d,g,h, respectively.

As indicated in Table 2 and Figure 6, the 1-mm-CCF/HDPE sample exhibited a low percolation threshold at DR 2 (Figure 9a), along with the highest t value at DR 2 and the lowest t value at DR 1 in Table 4. Hence, in the inflection region shown in Figure 9a, the DR 2 curve showed the most gradual change, whereas the DR 1 curve flattened at the fastest rate.

The fitted electrical conductivity curves and results of the least-squares fitting to obtain $\log \sigma_f$ and t for the 3 mm-CCF/HDPE

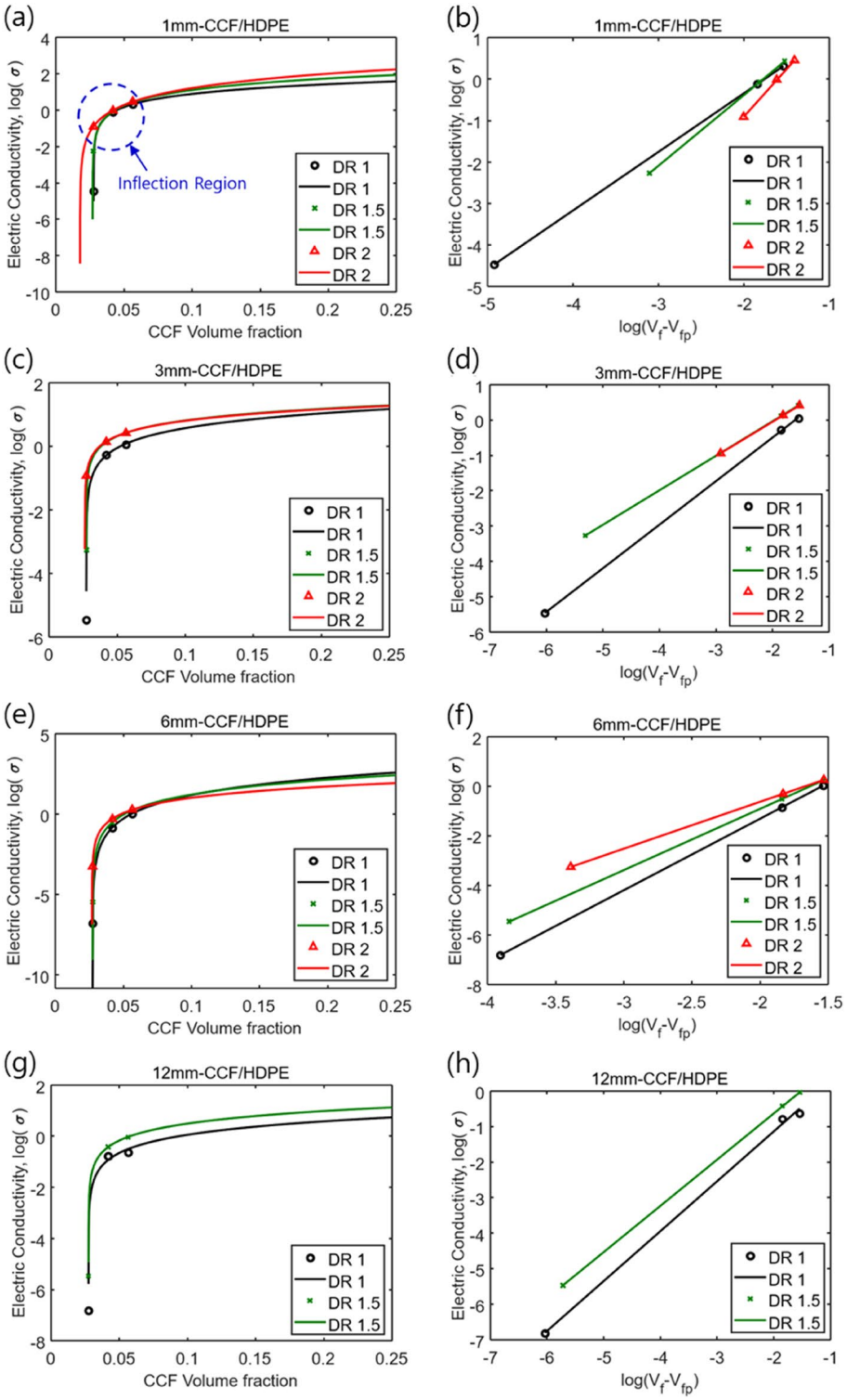

FIGURE 9 | Electrical conductivity versus CCF volume fraction of (a) 1, (c) 3, (e) 6, and (g) 12 mm-CCF/HDPE composites and least-squares fitting for $\log \sigma_f$ and t of (b) 1, (d) 3, (f) 6, and (h) 12 mm-CCF/HDPE composites (the dots expressed by circles, 'x's, and triangles in the graphs indicate the experimental results).

sample are shown in Figure 9c,d, respectively. As indicated in Table 2, the threshold values showed no significant difference. Therefore, no significant difference in the percolation threshold was observed, as shown in Figure 9c. The t value of DR 1 in Table 4 was the highest among the values for the 3-mm-CCF/HDPE. Consequently, the electrical conductivity for DR 1 increased more gradually and reached a plateau compared with that of DR 2 and 1.5 in the inflection region.

The electrical conductivity curves and results of the least-squares fitting for the 6-mm-CCF/HDPE sample are shown in Figure 9e,f, respectively. As indicated in Table 2, no significant

difference was observed in the percolation threshold depending on the DR for the 6 mm-CCF/HDPE sample, leading to the almost uniform threshold in Figure 9e. In the inflection region, the curve of DR 1 changed the least, whereas that of DR 2 changed the most rapidly. This discrepancy can be attributed to the large t value at DR 1 and small t value at DR 2 for the 6-mm-CCF sample, as indicated in Table 4.

The electrical conductivity curves and results of the least-squares fitting for the 12-mm-CCF/HDPE sample are shown in Figure 9g,h, respectively. Notably, this sample exhibited almost identical threshold values at DR 1 and 1.5 (Table 2), with a slightly smaller t value at DR 1 (Table 4).

As shown in Figure 9, the fitted electrical conductivity curves and results of the least-squares fitting align with the experimental results.

The electrical conductivity analysis results in terms of the DR are shown in Figure 10. In the case of DR 1 (Figure 10a), the percolation threshold V_{fp} exhibited an almost identical geometry. As shown in Table 2, the percolation threshold values for each sample were similar at DR 1. In the inflection region, the 12-mm-CCF/HDPE showed a rapid change, whereas the 6-mm-CCF/HDPE exhibited the mildest change. This discrepancy can be attributed to the lower t value of the 12-mm-CCF/HDPE sample compared with the higher t value of the 6 mm-CCF/HDPE sample, as indicated in Table 4. As mentioned previously, a rapid change in the inflection region was observed as t decreased, whereas a mild change was observed as t increased.

The difference in V_{fp} at DR 1.5 was insignificant, whereas the 3 and 12-mm-CCF/HDPE samples showed rapid changes in the inflection region. As indicated in Table 4, these samples had low t values.

In the case of DR 2, as discussed previously, the 1 mm-CCF/HDPE sample had a low percolation threshold value. As shown in Table 2, this sample exhibited the lowest value (V_{fp}: 0.017793). In addition, the 3 mm-CCF sample showed the most rapid change in the inflection region, whereas the 1-mm-CCF sample showed a more gradual change, as detailed in Table 4.

This study involved the analysis of electrical conductivity experimental results for CCF/HDPE composites, with the percolation theory results subjected to least-squares fitting. The overall findings indicate a strong agreement between the fitted percolation theory and experimental results.

TABLE 4 | t values obtained using least-squares fitting.

	1-mm CCF/ HDPE	3-mm CCF/ HDPE	6-mm CCF/ HDPE	12-mm CCF/ HDPE
DR 1	2.484779	1.962227	4.444364	1.651037
DR 1.5	3.037528	1.904026	4.014828	1.959796
DR 2	3.669626	1.880293	3.14051	—

4 | Conclusions

In this study, CCF/HDPE composite samples were prepared and analyzed based on the CCF content, CCF length, and DR. To achieve this, an alignment experiment of the CCF

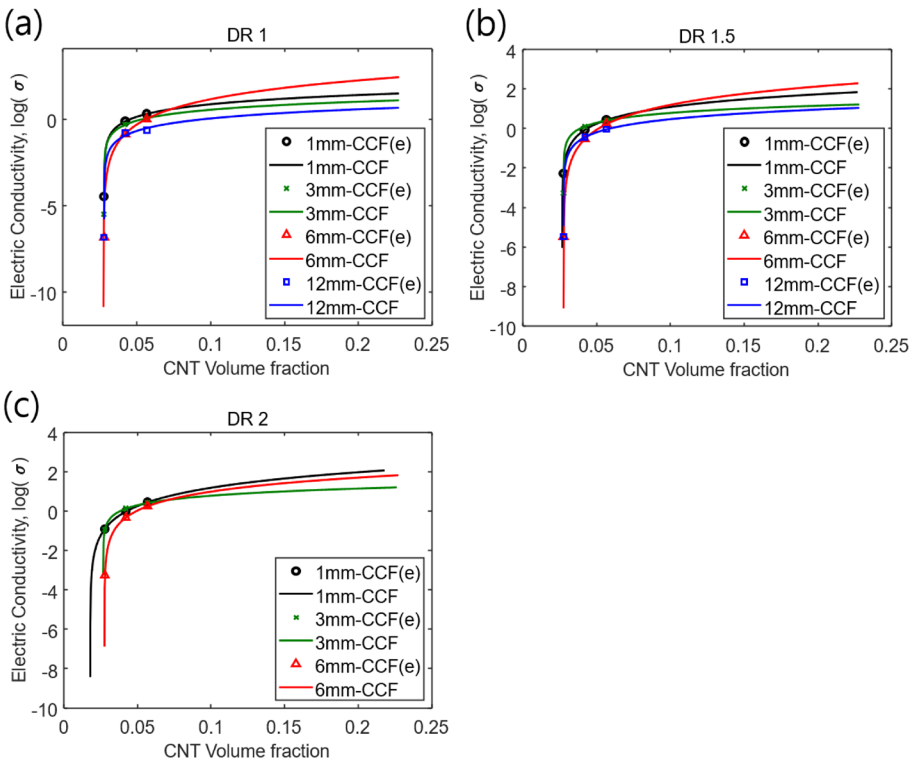

FIGURE 10 | Electrical conductivity curves of CCF/HDPE samples at DR 1, 1.5, and 2 ((e) indicates the experimental result).

was conducted through tensile loading following extrusion. The electrical conductivity increased with an increasing CCF content, a decreasing CCF length, and an increasing DR. The highest conductivity measured was 2.808 S/cm for CCF with a length of 1 mm, 10 wt%, and a DR of 2. For quantitative evaluation, the EMI shielding effectiveness (SE) was estimated based on the measured electrical conductivities, as described in Appendix C. The calculated SE values were approximately 52.9, 50.6, 41.9, and 29.8 dB for samples with different conductivities. These results suggest that the developed composites meet or exceed the typical EMI shielding requirements for automotive and electronic applications (see Table D1). The experimental results were further analyzed by fitting the percolation theory using the least-squares method. The percolation threshold decreased as the DR increased and CCF length decreased. A lower threshold signified higher electrical conductivity. In addition, the relationship between $\log \sigma_f$ and the DR varied among the different samples, with the 1mm-CCF/HDPE sample showing an increase in $log\sigma_f$ as the DR increased, whereas the other samples exhibited a decrease. Furthermore, the t value analysis revealed that the 1 and 6 mm-CCF/HDPE samples had higher values compared with the 3 and 12-mm-CCF/HDPE samples. A decrease in the t value corresponded to a rapid change in electrical conductivity within the inflection region. The fitted percolation theory exhibited excellent agreement with the experimental results. A rheological analysis is planned as future work to understand the flow behavior during processing further, which is expected to support the optimization of the extrusion process. Overall, the findings provide a foundation for the optimal design of conductive polymer composites.

Author Contributions

Gu-Hyeok Kang: conceptualization, methodology, software, data curation, investigation, formal analysis, visualization, writing – original draft, writing – review and editing. **Myungsoo Kim:** methodology, software, supervision, data curation, investigation, visualization, writing – original draft, writing – review and editing, funding acquisition, resources. **Young-Bin Park:** supervision, funding acquisition, writing – original draft, writing – review and editing, resources.

Acknowledgments

This research was supported by the K-Carbon Flagship R&D Program (grant no. RS-2024-00417957) funded by the Ministry of Trade, Industry and Energy (MOTIE) of Korea through the Korea Evaluation Institute of Industrial Technology (KEIT), by the National Research Foundation of Korea (NRF) funded by the Ministry of Science and ICT (MSIT) of Korea (grant no. 2021R1F1A1051836), by a National Research Council of Science and Technology (NST) grant funded by MSIT (grant no. CRC23011-000) and by the Korea Institute of Marine Science & Technology Promotion (KIMST) funded by the Ministry of Oceans and Fisheries (2520000449).

Conflicts of Interest

The authors declare no conflicts of interest.

Data Availability Statement

The data that support the findings of this study are available from the corresponding author upon reasonable request.

References

1. S. Sharma, V. Kumar, A. K. Pathak, et al., "Design of MWCNT Bucky Paper Reinforced PANI–DBSA–DVB Composites With Superior Electrical and Mechanical Properties," *Journal of Materials Chemistry C* 6, no. 45 (2018): 12396–12406.

2. Q. Jia, J. Li, L. Wang, J. Zhu, and M. Zheng, "Electrically Conductive Epoxy Resin Composites Containing Polyaniline With Different Morphologies," *Materials Science and Engineering A* 448, no. 1–2 (2007): 356–360.

3. T. Yokozeki, T. Goto, T. Takahashi, et al., "Development and Characterization of CFRP Using a Polyaniline-Based Conductive Thermoset Matrix," *Composites Science and Technology* 117 (2015): 277–281.

4. L. Vertuccio, L. Guadagno, G. Spinelli, et al., "Smart Coatings of Epoxy Based CNTs Designed to Meet Practical Expectations in Aeronautics," *Composites Part B: Engineering* 147 (2018): 42–46.

5. S. Das, S. Sharma, T. Yokozeki, and S. Dhakate, "Conductive Layer-Based Multifunctional Structural Composites for Electromagnetic Interference Shielding," *Composite Structures* 261 (2021): 113293.

6. S. Gong, Z. H. Zhu, M. Arjmand, U. Sundararaj, J. T. Yeow, and W. Zheng, "Effect of Carbon Nanotubes on Electromagnetic Interference Shielding of Carbon Fiber Reinforced Polymer Composites," *Polymer Composites* 39, no. S2 (2018): E655–E663.

7. S. Hu, D. Wang, J. Večerník, D. Křemenáková, and J. Militký, "Electromagnetic Interference (EMI) Shielding and Thermal Management of Sandwich-Structured Carbon Fiber-Reinforced Composite (CFRC) for Electric Vehicle Battery Casings," *Polymers* 16, no. 16 (2024): 2291.

8. J. U. Roh, D. J. Kwon, J. S. Guk, J. G. Kim, H. Y. Lee, and S. E. Park, "Evaluation of Mechanical Properties and EMI Shielding Effectiveness of Long Carbon Fiber Reinforced Thermoplastic With Different Matrix," *Journal of Composite Materials* 55, no. 6 (2021): 731–739.

9. P. A. Martinez, J. Victoria, J. Torres, et al., "Analysis of EMI Shielding Effectiveness for Plastic Fiber Composites in the 5G Sub-6 GHz Band," in *2021 IEEE International Joint EMC/SI/PI and EMC Europe Symposium* (IEEE, 2021), 278–283.

10. N. Duan, Z. Shi, J. Wang, G. Wang, and X. Zhang, "Strong and Flexible Carbon Fiber Fabric Reinforced Thermoplastic Polyurethane Composites for High-Performance EMI Shielding Applications," *Macromolecular Materials and Engineering* 305, no. 6 (2020): 1900829.

11. H. Liang, B. Du, Y. Zhao, S. Li, X. Zhang, and X. Chen, "Highly Efficient Inverse Lumped Modeling for the Pre-Strained Circular Dielectric Elastomer," *International Journal of Mechanical Sciences* 279 (2024): 109524.

12. W. Thongruang, R. J. Spontak, and C. M. Balik, "Correlated Electrical Conductivity and Mechanical Property Analysis of High-Density Polyethylene Filled With Graphite and Carbon Fiber," *Polymer* 43, no. 8 (2002): 2279–2286.

13. A. R. Ravindran, R. B. Ladani, S. Wu, A. J. Kinloch, C. H. Wang, and A. P. Mouritz, "The Electric Field Alignment of Short Carbon Fibres to Enhance the Toughness of Epoxy Composites," *Composites Part A: Applied Science and Manufacturing* 106 (2018): 11–23.

14. Q. Wu, J. Miao, W. Li, et al., "High-Performance Thermal Interface Materials With Magnetic Aligned Carbon Fibers," *Materials* 15, no. 3 (2022): 735.

15. Z. Liu, T. A. Turner, K. H. Wong, and S. J. Pickering, "Development of High Performance Recycled Carbon Fibre Composites With an Advanced Hydrodynamic Fibre Alignment Process," *Journal of Cleaner Production* 278 (2021): 123785.

16. H. Cheng, J. Zhou, L. Guo, H. Wang, and Z. Qian, "Dispersibility Optimization of Short Carbon Fiber Suspension for the Preparation of Carbon Fiber Aligned Mat Reinforced Composites," *Journal of Cleaner Production* 389 (2023): 136075.

17. D. Patidar and V. K. Pal, "Deformation Behaviour of Interconnect Encapsulated on Functionally Graded Stretchable Substrates," *International Journal of Mechanical Sciences* 257 (2023): 108539.

18. A. K. Mohanty, S. Vivekanandhan, N. Tripathi, et al., "Sustainable Composites for Lightweight and Flame Retardant Parts for Electric Vehicles to Boost Climate Benefits: A Perspective," *Composites Part C: Open Access* 12 (2023): 100380.

19. H.-J. Um, Y.-T. Hwang, I.-J. Bae, and H.-S. Kim, "Design and Manufacture of Thermoplastic Carbon Fiber/Polyethylene Terephthalate Composites Underbody Shield to Protect the Lithium-Ion Batteries for Electric Mobility From Ground Impact," *Composites Part B: Engineering* 238 (2022): 109892.

20. Z. Cui, Q. Liu, Y. Sun, and Q. Li, "On Crushing Responses of Filament Winding CFRP/Aluminum and GFRP/CFRP/Aluminum Hybrid Structures," *Composites Part B: Engineering* 200 (2020): 108341.

21. T. B. Nieduzak, E. M. Tronci, T. Zhou, L. B. Demo, M. Q. Feng, and V. Aitharaju, "Heat Transfer Model for Temperature-Sensing Polymer Composite EV Battery Enclosure," *Composites Part B: Engineering* 296 (2025): 112258.

22. S. Ronca, T. Igarashi, G. Forte, and S. Rastogi, "Metallic-Like Thermal Conductivity in a Lightweight Insulator: Solid-State Processed Ultra High Molecular Weight Polyethylene Tapes and Films," *Polymer* 123 (2017): 203–210.

23. S. N. Wei, X. Liu, J. Yan, et al., "A Study of the Mechanical Performance of Nanocomposites of Polyethylene Containing Exfoliated Boron Nitride Nanoplatelets," *Polymer Composites* 43, no. 9 (2022): 6276–6286.

24. S. Baskut and S. Turan, "The Effect of Different GNPs Addition on the Electrical Conductivities and Percolation Thresholds of the SiAlON Matrix Composites," *Journal of the European Ceramic Society* 40, no. 4 (2020): 1159–1167.

25. G. Pinto and A. K. Maaroufi, "Nonlinear Electrical Conductivity of Tin-Filled Urea-Formaldehyde-Cellulose Composites," *Polymer Composites* 26, no. 3 (2005): 401–406.

26. G. Pinto, A. K. Maaroufi, R. Benavente, and J. M. Pereña, "Electrical Conductivity of Urea–Formaldehyde–Cellulose Composites Loaded With Copper," *Polymer Composites* 32, no. 2 (2011): 193–198.

27. H. Im, S. Yun, and J. Kim, "Electro Conductivities of Well-Dispersed PMMA-g-MWNTs/6FDA-Based Polyimide Composites: Effect of Chemical Structure," *Polymer Composites* 32, no. 3 (2011): 368–377.

28. Q. Zhang, H. Xiong, W. Yan, D. Chen, and M. Zhu, "Electrical Conductivity and Rheological Behavior of Multiphase Polymer Composites Containing Conducting Carbon Black," *Polymer Engineering & Science* 48, no. 11 (2008): 2090–2097.

29. E. Mamunya, V. Davidenko, and E. Lebedev, "Percolation Conductivity of Polymer Composites Filled With Dispersed Conductive Filler," *Polymer Composites* 16, no. 4 (1995): 319–324.

30. A. Celzard, G. Furdin, J. Mareche, E. McRae, M. Dufort, and C. Deleuze, "Anisotropic Percolation in an Epoxy-Graphite Disc Composite," *Solid State Communications* 92, no. 5 (1994): 377–383.

31. M. B. Heaney, "Measurement and Interpretation of Nonuniversal Critical Exponents in Disordered Conductor–Insulator Composites," *Physical Review B* 52, no. 17 (1995): 12477–12480.

32. Y. P. Mamunya, Y. V. Muzychenko, P. Pissis, E. Lebedev, and M. Shut, "Processing, Structure, and Electrical Properties of Metal-Filled Polymers," *Journal of Macromolecular Science, Part B* 40, no. 3–4 (2001): 591–602.

33. G.-H. Kang, M. Kim, and Y.-B. Park, "Improvement of Electrical Conductivity in Glass Bubble-Carbon Nanotube/Polyamide 6 Hybrid Scale Composite Through Novel Mechanical Forming and Segregated Network Morphology," *Polymer Testing* 126 (2023): 108138.

34. M. Kim, G.-H. Kang, H. W. Park, Y.-B. Park, Y. H. Park, and K. H. Yoon, "Design, Manufacturing, and Characterization of High-Performance Lightweight Bipolar Plates Based on Carbon Nanotube-Exfoliated Graphite Nanoplatelet Hybrid Nanocomposites," *Journal of Nanomaterials* 2012, no. 1 (2012): 159737.

35. E. T. Thostenson and T.-W. Chou, "On the Elastic Properties of Carbon Nanotube-Based Composites: Modelling and Characterization," *Journal of Physics D: Applied Physics* 36, no. 5 (2003): 573–582.

36. V. Chenrayan, C. Manivannan, K. Shahapurkar, et al., "An Experimental and Empirical Assessment of Machining Damage of Hybrid Glass-Carbon FRP Composite During Abrasive Water Jet Machining," *Journal of Materials Research and Technology* 19 (2022): 1148–1161.

37. K. Shahapurkar, C. Venkatesh, M. R, et al., "Influence of Graphene Nano Fillers and Carbon Nano Tubes on the Mechanical and Thermal Properties of Hollow Glass Microsphere Epoxy Composites," *PRO* 10, no. 1 (2021): 40.

38. P. Pötschke, T. Fornes, and D. Paul, "Rheological Behavior of Multiwalled Carbon Nanotube/Polycarbonate Composites," *Polymer* 43, no. 11 (2002): 3247–3255.

39. J. Thomasset, P. J. Carreau, B. Sanschagrin, and G. Ausias, "Rheological Properties of Long Glass Fiber Filled Polypropylene," *Journal of Non-Newtonian Fluid Mechanics* 125, no. 1 (2005): 25–34.

40. J. H. Jeon, C. K. Yoon, Y.-J. Quan, et al., "Effect of Fiber Entanglement in Chopped Glass Fiber Reinforced Composite Manufactured via Long Fiber Spray-Up Molding," *Heliyon* 9, no. 12 (2023): e22170.

Appendix A

Table A1 shows the electrical conductivity of 1 mm-CCF/HDPE composites and the normalized values for the conductivity. As the electrical conductivity value varied significantly depending on the DR, it was normalized for easy comparison. During the normalization process, the electrical conductivity for 5 and 7.5 wt% was divided by the 10 wt% conductivity of the CCF/HDPE sample, which was the highest conductivity value, as shown in Table A1. In addition, Figure 4a was obtained using the average values of the normalized values. The graphs of the 3, 6, and 12-mm-CCF/HDPE composites in Figure 4a were obtained using the averages of the normalized values in Tables A2–A4, respectively. The graph in Fig. 4c was obtained using the averages of the normalized values. The graphs of the 3 and 6 mm-CCF/HDPE composites in Fig. 4c were obtained using Tables A2 and A3, respectively. As there was no experimental result for the 12 mm-CCF/HDPE at DR 2, the normalization was performed based on the electrical conductivity of DR 1.5 (Table A4).

TABLE A1 | Electrical conductivities of 1-mm-CCF/HDPE composites and normalized values.

		2.5 wt%	5 wt%	7.5 wt%	10 wt%
Original conductivity (S/cm)	DR 1	0	3.3500E-05	0.7590	2.0448
	DR 1.5	0	5.3500E-03	0.8386	2.6760
	DR 2	0	1.2291E-01	0.9514	2.8079
Normalized conductivity	DR 1	0	1.6383E-05	0.3712	1
	DR 1.5	0	1.9993E-03	0.3134	1
	DR 2	0	4.3772E-02	0.3388	1
	Average	0	1.5263E-02	0.3411	1

TABLE A2 | Electrical conductivities of 3-mm-CCF/HDPE composites and normalized values.

		2.5 wt%	5 wt%	7.5 wt%	10 wt%
Original conductivity (S/cm)	DR 1	0	3.3500E-06	0.5167	1.10243
	DR 1.5	0	5.3500E-04	1.2756	2.54042
	DR 2	0	1.1425E-01	1.3465	2.56295
Normalized conductivity	DR 1	0	3.0387E-06	0.4687	1
	DR 1.5	0	2.1060E-04	0.5021	1
	DR 2	0	4.4578E-02	0.5254	1
	Average	0	1.4930E-02	0.4987	1

TABLE A3 | Electrical conductivities of 6-mm-CCF/HDPE composites and normalized values.

		2.5 wt%	5 wt%	7.5 wt%	10 wt%
Original conductivity (S/cm)	DR 1	0	1.5200E-07	0.1368	1.0325
	DR 1.5	0	3.3500E-06	0.2940	1.6585
	DR 2	0	5.3500E-04	0.4729	1.7489
Normalized conductivity	DR 1	0	1.4722E-07	0.1325	1
	DR 1.5	0	2.0200E-06	0.1773	1
	DR 2	0	3.0591E-04	0.2704	1
	Average	0	1.0269E-04	0.1934	1

TABLE A4 | Electrical conductivities of 12-mm-CCF/HDPE composites and normalized values.

		2.5 wt%	5 wt%	7.5 wt%	10 wt%
Original conductivity (S/cm)	DR 1	0	1.5200E-07	0.1617	0.2282
	DR 1.5	0	3.3500E-06	0.3708	0.8941
	DR 2	—	—	—	—
Normalized conductivity	DR 1	0	6.6611E-07	0.7088	1
	DR 1.5	0	3.7470E-06	0.4147	1
	DR 2	—	—	—	—
	Average	0	2.2065E-06	0.5617	1

Appendix B

Table B1 shows the electrical conductivity of the CCF/HDPE composites manufactured at DR 1 and the normalized values for the conductivity. The electrical conductivity values were normalized by dividing them by the value of the 1-mm-CCF/HDPE sample, which had the highest electrical conductivity. In addition, the graph in Figure 4b was obtained using the average of the normalized values. The graphs for DR 1.5 and 2 in Figure 4b were obtained using Tables B2 and B3, respectively.

TABLE B1 | Electrical conductivities of CCF/HDPE composites with DR 1 and normalized values.

		1 mm	3 mm	6 mm	12 mm
Original conductivity (S/cm)	5 wt%	3.350E-05	3.350E-06	1.520E-07	1.520E-07
	7.5 wt%	0.7590	0.5167	0.1368	0.1617
	10 wt%	2.0448	1.1024	1.0325	0.2282
Normalized conductivity	5 wt%	1	0.1	0.0045	0.0045
	7.5 wt%	1	0.6808	0.1802	0.2131
	10 wt%	1	0.5391	0.5049	0.1116
	Average	1	0.4400	0.2299	0.1097

TABLE B2 | Electrical conductivities of CCF/HDPE composites with DR 1.5 and normalized values.

		1 mm	3 mm	6 mm	12 mm
Original conductivity (S/cm)	5 wt%	5.350E-03	5.350E-04	3.350E-06	3.350E-06
	7.5 wt%	0.8386	1.2756	0.29401	0.37076
	10 wt%	2.6760	2.5404	1.65845	0.89406
Normalized conductivity	5 wt%	1	0.1	6.262E-04	6.262E-04
	7.5 wt%	1	1.5212	0.3506	0.4421
	10 wt%	1	0.9493	0.6198	0.3341
	Average	1	0.8568	0.3237	0.2590

TABLE B3 | Electrical conductivities of CCF/HDPE composites with DR 2 and normalized values.

		1 mm	3 mm	6 mm	12 mm
Original conductivity (S/cm)	5 wt%	0.1229	0.1143	5.350E-04	—
	7.5 wt%	0.9514	1.3465	0.4729	—
	10 wt%	2.8079	2.5630	1.7489	—
Normalized conductivity	5 wt%	1	0.9295	4.353E-03	—
	7.5 wt%	1	1.4152	0.4971	—
	10 wt%	1	0.9128	0.6228	—
	Average	1	1.0858	0.3748	—

Appendix C

Estimation of SE

To support the practical relevance of this study, the SE of the CCF/HDPE composites was estimated using a simplified absorption-dominated model. The equation is as follows:

Simplified absorption-dominated SE model:

$$\mathrm{SE} \approx 8.68 \cdot t \cdot \sqrt{\pi f \mu \sigma}$$

where SE: shielding effectiveness (dB); t: material thickness (cm); f: frequency (Hz); μ: magnetic permeability (H/m); σ: electrical conductivity (S/m).

The calculated SE values were approximately 52.9, 50.6, 41.9, and 29.8 dB, corresponding to the maximum electrical conductivity values for each CCF length, assuming a material thickness of 2 cm and a magnetic permeability of $4\pi \times 10^{-7}$ H/m. These results demonstrate that the developed composites exhibit promising EMI shielding performance, meeting the typical requirements for potential automotive and electronic applications.

Appendix D

Typical EMI Shielding Requirements

TABLE D1 | Typical EMI shielding requirements for automotive components.

Application area	Frequency range	Required SE
ECU, ABS, ETC	1 MHz–1 GHz	≥ 40 dB
Infotainment systems, ADAS	30 MHz–6 GHz	≥ 50 dB
High-voltage battery systems	10 MHz–2.5 GHz	≥ 60 dB
High-speed data lines	MHz to GHz	≥ 40–60 dB
Radar, cameras, and sensor modules	~76 GHz (automotive radar)	≥ 30 dB (a lower SE may be acceptable)